a suspension of dead *E. coli* (OP50) placed on the agar medium. Briefly, daumone-containing plates (5 mm diameter) were prepared with 3 ml NGM (without peptone) as described, and known amounts of *E. coli* suspension that had been heated at 95 °C for 30 min (with vigorous vortexing every 5 min) were added. Separately, a daumone stock solution was prepared by dissolving daumone in ethanol (320 μg in 150 μl) then adding 150 μl double-distilled water to make a final solution of 320 μg in 300 μl. This daumone solution was evenly spread over the plate and allowed to dry in a clean hood. Once plates were dry, dead *E. coli* were loaded onto the center of the plate at a concentration of 160 μg per 20 μl. Plates were left to dry for an hour, then stored at 4 °C until use for dauer-formation assays.

For the dauer-formation assay, five adult *C. elegans* were placed on a plate and incubated at 20 °C for 4–6 h. After incubation, adult worms were removed and the eggs on the plate (generally 50–100 eggs per plate) were incubated for 52–72 h and then counted. A 1% SDS solution (1.0 ml) was added to the plate and the surviving worms were counted as dauer larvae. For Sudan-black staining of fat storage in the dauer larvae, worms were fixed with 1% paraformaldehyde, washed, dehydrated with ethanol and stained with dye[19].

NMR analysis

For NMR experiments, the compound (~1 mg) was dissolved in deuterated methanol at a concentration of 30 mg ml^{-1}, and spectra were acquired at 25 °C with a Bruker DRX 500 MHz spectrometer. In the 2D-NMR experiments, the ^{1}H chemical shifts were referenced to internal sodium 4,4-dimethyl-4-silapentane-1-sulphonate (DSS). For ^{1}H-^{1}H 2D-DQF-COSY[20], ^{1}H-^{1}H 2D-TOCSY and ^{1}H-^{1}H 2D-ROESY experiments[21], data were collected using a 7,002.80 Hz spectral width, 2,048 complex points in t_2 and 128 increments in t_1. ^{13}C-HMQC[22,23] and ^{13}C-HMBC[24] spectra were recorded for the assignment of carbon and proton resonances[25]. Proton and carbon resonances of daumone were easily assigned using the combined techniques of DEPT, HMQC, HMBC, and DQF-COSY NMR (see Supplementary Information).

Total chemical synthesis and stereospecific structure determination

A detailed description of the chemical synthesis process is described in the Supplementary Information. The synthesized compound was identified as a synthetic daumone using the established dauer-formation assay described above. The stereospecific structure of the compound was also confirmed to be identical to the natural daumone. Please refer to the Supplementary Information for experimental procedures regarding the synthesis of daumone and its intermediates (**3**, **4**, **5**, **8**, **10**, **11**, **12** and **1**), spectral data for the synthetic daumone (including ^{1}H NMR, ^{13}C NMR, Fourier transform infared spectroscopy (FTIR), HRMS (fast atom bombardment), DEPT, HMBC, NOESY, ROESY, high-resolution Q-TOF mass spectrometry and retention factor (R_f)) and elemental analysis data for the synthetic daumone.

1. Cassada, R. C. & Russell, R. L. The dauer larva, a post-embryonic developmental variant of the nematode *Caenorhabditis elegans*. *Dev. Biol.* **46**, 326–342 (1975).
2. Golden, J. W. & Riddle, D. L. A pheromone influences larval development in the nematode *Caenorhabditis elegans*. *Science* **218**, 578–580 (1982).
3. Golden, J. W. & Riddle, D. L. The *Caenorhabditis elegans* dauer larva: developmental effects of pheromone, food, and temperature. *Dev. Biol.* **102**, 368–378 (1984).
4. Golden, J. W. & Riddle, D. L. A *Caenorhabditis elegans* dauer-inducing pheromone and an antagonistic component of the food supply. *J. Chem. Ecol.* **10**, 1265–1280 (1984).
5. Bargmann, C. I. & Horvitz, H. R. Control of larval development by chemosensory neurons in *Caenorhabditis elegans*. *Science* **251**, 1243–1246 (1991).
6. Schackwitz, W. S., Inoue, T. & Thomas, J. H. Chemosensory neurons function in parallel to mediate a pheromone response in *C. elegans*. *Neuron* **17**, 719–728 (1996).
7. Thomas, J. H., Birnby, D. A. & Vowels, J. J. Evidence for parallel processing of sensory information controlling dauer formation in *Caenorhabditis elegans*. *Genetics* **134**, 1105–1117 (1993).
8. Patterson, G. I., Koweek, A., Wong, A., Liu, Y. & Ruvkun, G. The DAF-3 Smad protein antagonizes TGF-beta-related receptor signaling in the *Caenorhabditis elegans* dauer pathway. *Genes Dev.* **11**, 2679–2690 (1997).
9. Apfeld, J. & Kenyon, C. Regulation of lifespan by sensory perception in *Caenorhabditis elegans*. *Nature* **402**, 804–809 (1999).
10. Perkins, L. A., Hedgecock, E. M., Thomson, J. N. & Culotii, J. G. Mutant sensory cilia in the nematode *Caenorhabditis elegans*. *Dev. Biol.* **117**, 456–487 (1986).
11. Antebi, A., Culotti, J. G. & Hedgecock, E. M. daf-12 regulates developmental age and the dauer alternative in *Caenorhabditis elegans*. *Development* **125**, 1191–1205 (1998).
12. Bird, D. M. & Opperman, C. H. *Caenorhabditis elegans*: A genetic guide to parasitic nematode biology. *J. Nematol.* **30**, 299–308 (1998).
13. Viney, M. E. & Franks, N. R. Is dauer pheromone of *Caenorhabditis elegans* really a pheromone? *Naturwissenschaften* **91**, 123–124 (2004).
14. Regnier, F. E. & Law, J. H. Insect pheromone. *J. Lipid Res.* **9**, 541–551 (1968).
15. Koga, M., Take-uchi, M., Tameishi, T. & Ohshima, Y. Control of DAF-7 TGF-(alpha) expression and neuronal process development by a receptor tyrosine kinase KIN-8 in *Caenorhabditis elegans*. *Development* **126**, 5387–5398 (1999).
16. Brenner, S. The genetics of *Caenorhabditis elegans*. *Genetics* **77**, 71–94 (1974).
17. Choi, B. K., Chitwood, D. J. & Paik, Y.-K. Proteomic changes during disturbance of cholesterol metabolism by azacoprostane treatment in *Caenorhabditis elegans*. *Mol. Cell. Proteomics* **2**, 1086–1095 (2003).
18. Vowels, J. J. & Thomas, J. H. Multiple chemosensory defects in daf-11 and daf-21 mutants of *Caenorhabditis elegans*. *Genetics* **138**, 303–316 (1994).
19. Kimura, K. D., Tissenbaum, H. A., Liu, Y. & Ruvkun, G. daf-2, an insulin receptor-like gene that regulates longevity and diapause in *Caenorhabditis elegans*. *Science* **277**, 942–946 (1997).
20. Rance, M. *et al.* Improved spectral resolution in cosy 1H NMR spectra of proteins via double quantum filtering. *Biochem. Biophys. Res. Commun.* **117**, 479–485 (1983).
21. Bax, A. & Subramanian, S. Sensitivity-enhanced two-dimensional heteronuclear shift correlation NMR spectroscopy. *J. Magn. Reson.* **67**, 565–570 (1986).
22. Bax, A. & Davis, D. G. Practical aspects of two-dimensional transverse NOE spectroscopy. *J. Magn. Reson.* **63**, 207–213 (1985).
23. Bax, A., Griffey, R. H. & Hawkins, B. L. Correlation of proton and nitrogen-15 chemical shifts by multiple quantum NMR. *J. Magn. Reson.* **55**, 301–315 (1983).
24. Bax, A. & Summers, M. F. ^{1}H and ^{13}C assignments from sensitivity enhanced detection of heteronuclear multiple-bond connectivity by two-dimensional multiple quantum NMR. *J. Am. Chem. Soc.* **108**, 2093–2094 (1986).
25. Schleucher, J. *et al.* A general enhancement scheme in heteronuclear multidimensional NMR employing pulsed field gradients. *J. Biomol. NMR* **4**, 301–306 (1994).

....

Structure and different conformational states of native AMPA receptor complexes

Terunaga Nakagawa[1], **Yifan Cheng**[2], **Elizabeth Ramm**[1], **Morgan Sheng**[1] **& Thomas Walz**[2]

[1]*The Picower Center for Learning and Memory, RIKEN-MIT Neuroscience Research Center, Howard Hughes Medical Institute, Massachusetts Institute of Technology, 77 Massachusetts Avenue, Cambridge, Massachusetts 02139, USA*
[2]*Department of Cell Biology, Harvard Medical School, 240 Longwood Avenue, Boston, Massachusetts 02115, USA*

....

Ionotropic glutamate receptors mediate fast excitatory synaptic transmission in the central nervous system[1,2]. Their modulation is believed to affect learning and memory, and their dysfunction has been implicated in the pathogenesis of neurological and psychiatric diseases[1,2]. Despite a wealth of functional data, little is known about the intact, three-dimensional structure of these ligand-gated ion channels. Here, we present the structure of native AMPA receptors (α-amino-3-hydroxy-5-methyl-4-isoxazole propionic acid; AMPA-Rs) purified from rat brain, as determined by single-particle electron microscopy. Unlike the homotetrameric recombinant GluR2 (ref. 3), the native hetero-tetrameric AMPA-R adopted various conformations, which reflect primarily a variable separation of the two dimeric extra-cellular amino-terminal domains. Members of the stargazin/ TARP family of transmembrane proteins co-purified with AMPA-Rs and contributed to the density representing the transmembrane region of the complex. Glutamate and cyclothiazide markedly altered the conformational equilibrium of the channel complex, suggesting that desensitization is related to separation of the N-terminal domains. These data provide a glimpse of the conformational changes of an important ligand-gated ion channel of the brain.

Ionotropic glutamate receptors include the NMDA (*N*-methyl-D-aspartate)-, AMPA- and kainate-preferring receptor channels. AMPA-Rs conduct most of the fast excitatory postsynaptic current (EPSC), and their regulation is critical for synaptic plasticity[1]. GluR1–4 (also known as GluR-A–D) encode subunits of

mammalian AMPA-Rs and have similar primary structures[4,5].

AMPA-R subunits consist of an N-terminal domain (NTD), a ligand-binding domain (LBD), a transmembrane domain (TMD) and a short, intracellular carboxy-terminal tail (Fig. 1a). The channel-forming TMD contains three membrane-spanning segments (M1, M3, M4) and the M2 "re-entrant loop"[2]. AMPA-Rs have been proposed to have a heterotetrameric, dimer-of-dimers organization[6–12]; however, the complex membrane topology and the heteromeric nature of AMPA-Rs hinder accurate structural modelling of the entire receptor[13–15].

To investigate its intact structure, native AMPA-Rs were purified from CHAPS-solubilized rat brain synaptosomes in the presence of the antagonist NBQX (2,3-dioxo-6-nitro-1,2,3,4-tetrahydrobenzo[f]quinoxaline-7-sulphonamide; added to block the effect on AMPA-R of endogenous glutamate, and removed during the final gel filtration chromatography step; Supplementary Fig. 1a). In negative stain electron microscopy images, the AMPA-Rs were monodispersed and homogeneous in size, but had various shapes (Fig. 1b). The AMPA-R particles were further analysed by multi-variate statistical analysis, classification and multi-reference alignment. The most common class averages (Fig. 1b, insets 1–3) show a strong but featureless oblong density in the bottom, with two elongated bipartite densities asymmetrically stacked on top of it. An additional, less-well-defined density lies between the oblong domain and the two bipartite densities.

Antigen-binding fragments (Fab) that recognize the C terminus of GluR1 or GluR2 decorated the lower part of the large oblong density (Fig. 1c, e). Fab fragments that recognize the NTD of GluR1 consistently bound to the two elongated bipartite densities, which we interpret as NTD dimers (Fig. 1d). Because the C-terminal tail is small and extends from M4, the Fab labelling implies that the oblong density represents the TMD (Fig. 1a, f). The weaker density between the TMD and the NTDs probably corresponds to the LBDs (Fig. 1a, f).

Other class averages showed a 'V'-shaped conformation with a pseudo-two-fold symmetry (Fig. 1b, insets 4 and 5). In these particles the two NTD densities are separated and positioned at varying angles relative to the TMD. Recognition by all three Fab fragments suggests that these V-shaped particles are also AMPA-Rs (Fig. 1c–e, far-right panels).

To calculate three-dimensional maps we prepared AMPA-Rs by cryo-negative staining[16] and recorded image pairs of specimens tilted to 50° and 0°. The images of the untilted specimens were used to classify the particles according to their shape, and the images of the tilted specimens were then used to calculate three-dimensional reconstructions of individual classes using the random conical tilt approach[17].

Density maps of three different classes of particles at a resolution of ~40 Å reveal distinct conformations of the AMPA-Rs (Fig. 2a, b). Re-projections from the density maps are almost identical to the class averages, demonstrating the consistency of the three-dimensional reconstructions with the projections (Fig. 2a, b, compare left and right panels; see also Supplementary Figs 2 and 3). Statistics for the three-dimensional reconstructions are summarized in Table 1. Depending on whether the NTDs are partially overlapping (Fig. 2a) or separated (Fig. 2b), we will refer to AMPA-Rs as adopting either a type I or type II conformation, respectively.

The NTDs are homologous to the bacterial periplasmic amino-acid-binding protein LIVBP and to the extracellular (ligand binding) domain of metabotropic glutamate receptors (mGluRs). Consistent with the proposed dimer-of-dimers organization of AMPA-Rs, the volume of the extracellular domain in our density map can accommodate two dimeric crystal structures of the mGluR1 extracellular domain[18] (with some extra amino acids removed; see Supplementary Fig. 4) and two dimeric crystal structures of the GluR2 LBD[19,20]. Placing of the crystal structures into our three-dimensional reconstruction (Fig. 2c) demonstrates that the size and

shape of the densities representing the extracellular AMPA-R domains are compatible with the known crystal structures. Owing to the limited resolution of our electron microscopy map, we did not refine the fit using computational algorithms. The M1–M3 membrane segments of GluRs are related to the KcsA K^+ channel, although in an inverted orientation[2,8]. The volume of the crystal structure of the KcsA channel core[21] was insufficient to occupy completely the transmembrane density of our structure (Fig. 2c).

When purified AMPA-Rs were concentrated and re-examined by SDS–polyacrylamide gel electrophoresis (PAGE), we detected two additional clusters of diffuse bands centred at ~50 and ~35 kDa (Fig. 3a). Mass spectrometry (liquid chromatography tandem mass spectrometry) of these bands identified proteins of the stargazin/TARP (transmembrane AMPA-R regulatory protein) family[22], specifically γ-2/stargazin (36 kDa), γ-3 (36 kDa), γ-4 (37 kDa) and γ-8 (43 kDa)[23] (Supplementary Table 1). TARPs are transmembrane proteins with four membrane-spanning segments that interact with AMPA-Rs and are critical for AMPA-R targeting to synapses in cerebellar granule cells[22]. Immunoblotting confirmed their presence in the preparation (Fig. 3b).

TARPs were largely removed when purified AMPA-Rs were subjected to gel filtration in the presence of decyl maltoside and dodecyl maltoside, slightly stronger detergents than CHAPS (Fig. 3b, c). Class averages of AMPA-Rs in dodecyl maltoside showed a substantially smaller transmembrane density (Fig. 3d, right panels) than those obtained in CHAPS (Fig. 3d, left panels). Moreover, anti-TARP Fab fragments specifically labelled the TMD of AMPA-Rs purified in CHAPS (Fig. 3e). Thus, TARPs contribute
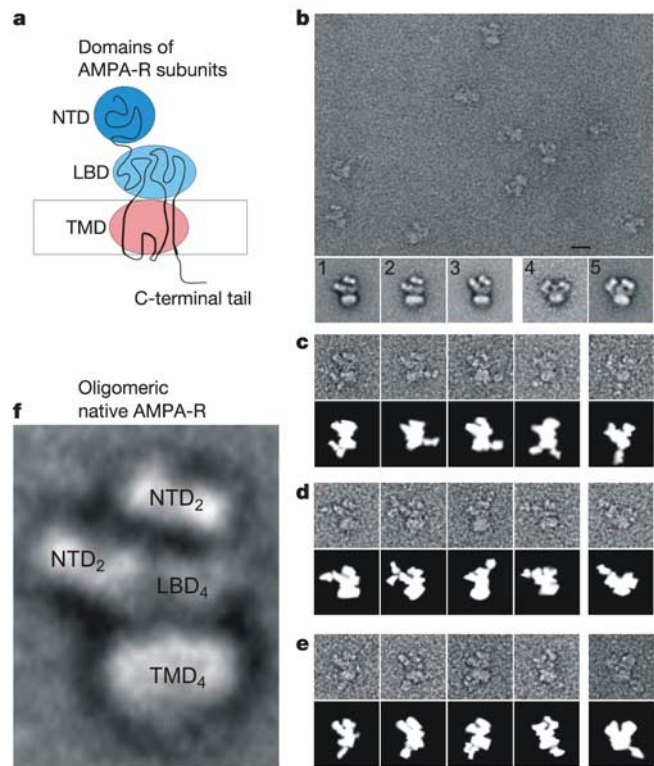

Figure 1 Negative staining and Fab decoration of AMPA-Rs. **a**, Domain organization of a GluR subunit. **b**, Negatively stained AMPA-Rs and representative class averages. Scale bar, 20 nm. The size of panels 1–5 is 40 × 40 nm. **c–e**, Labelling with Fab fragments against C-terminal peptide of GluR1 (**c**), NTD of GluR1 (**d**) and C-terminal peptide of GluR2 (**e**). Upper rows: raw particle images; lower rows: schematic representations. The size of individual panels is 40 × 40 nm. **f**, Assignment of projection densities to domains of AMPA-R subunits from **a**. NTD₂, NTD dimers; LBD₄, four LBDs; TMD₄, tetrameric TMD.
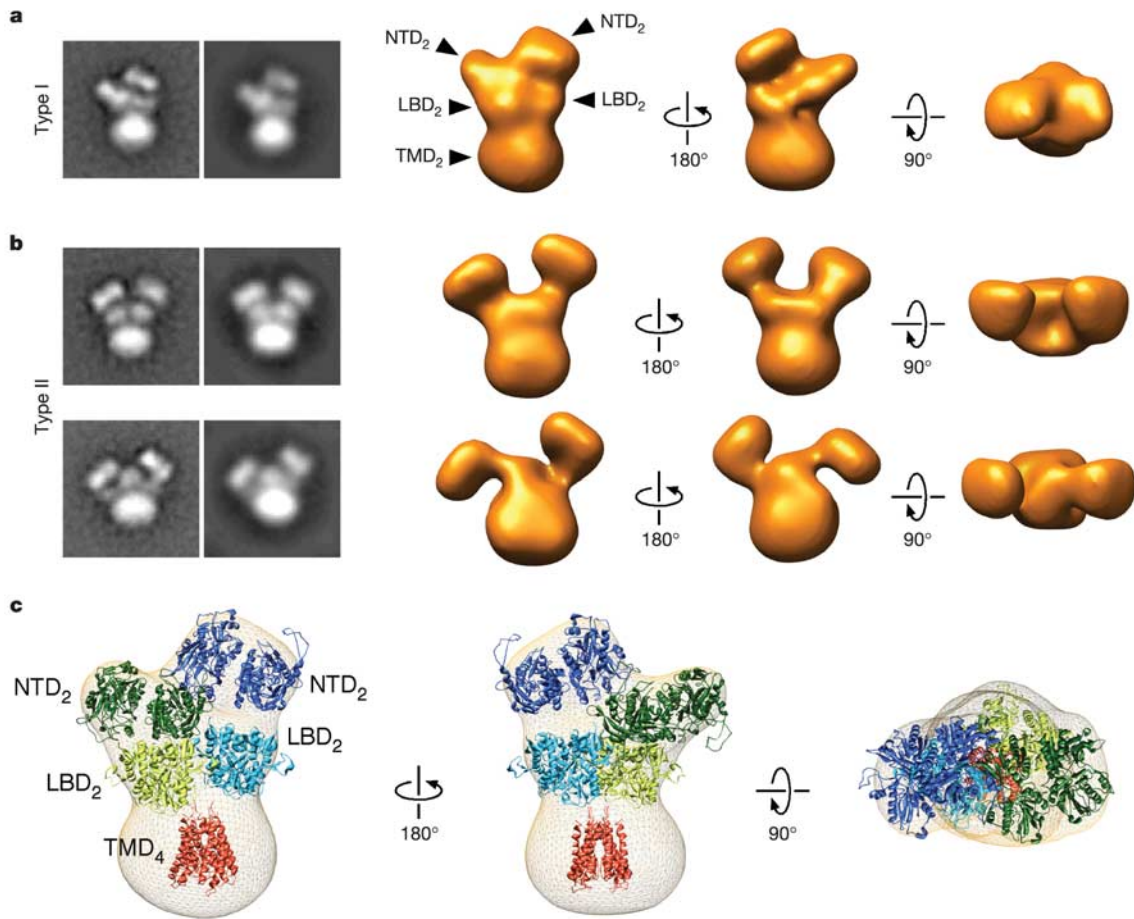
Figure 2 Three-dimensional reconstruction of AMPA-Rs and placement of crystal structures into the density map. **a**, Comparison of class average (left panel) and re-projection from the three-dimensional map (right panel), and views of the three-dimensional map of AMPA-R in the type I conformation. NTD_2 and LBD_2 indicate dimers, and TMD_4 indicates the tetrameric TMD. **b**, Same as **a** for AMPA-Rs in the type II conformation. Thresholds of all the electron microscopy densities were set at 5.3 sigma.

c, Placement of known crystal structures into the electron microscopy density map for type I AMPA-R. The crystal structures used are: extracellular domain of mGluR1 (Protein Data Bank 1EWV; dark blue and dark green); ligand-binding domain of GluR2 (Protein Data Bank 1LBC; light blue and light green); and transmembrane segment of KcsA (Protein Data Bank 1BL8; red).

to the transmembrane density of native AMPA-R complexes.

TARPs were reported to dissociate from AMPA-Rs upon binding of glutamate[23]. However, in our preparation TARPs remained bound to AMPA-Rs when the CHAPS-solubilized complex was treated with 3 mM glutamate (effector concentration for half-maximum response (EC_{50}) = 500 μM) (Fig. 3b), suggesting that additional factors are required for dissociation of TARPs from AMPA-Rs.

When glutamate binds to AMPA-R the channel opens but closes again after a few milliseconds, despite continued exposure to the ligand. Such desensitization is a feature of many receptors and ion channels. Cyclothiazide prevents desensitization of AMPA-Rs[20,24]

and locks them in the open-channel state. To test for possible effects on the conformation, we treated the same AMPA-R preparation with glutamate and/or cyclothiazide (Fig. 4). Approximately 10,000 negatively stained particles were classified into 100 classes by multivariate statistical analysis and multi-reference alignment. We then assigned each class average (and the particles in these classes) either to type I or II (Fig. 4d). Classes that could not be assigned unambiguously to one of the two conformations were termed 'unclassifiable' (see Supplementary Fig. 5 for all the assignments and Fig. 4e for the summary). In untreated AMPA-R preparations (Fig. 4a), ~60% of classifiable particles were of type I, whereas ~40% were type II. This ratio changed markedly in the presence of

Conformation type	Picked particles	Particles used for two-dimensional classification	Particles used in final three-dimensional reconstruction	Resolution (Å) at FSC = 0.5	Resolution (Å) at FSC = 0.142	Volume (nm³) at × 5.3 sigma
Type I	24,831 pairs	21,291	1,206	42	31	1,151
Type IIa*	38,971 pairs	27,573	956	46	33	1,137
Type IIb†	38,971 pairs	27,573	1,593	42	31	1,087

Table 1 Statistics of the three-dimensional reconstructions

Type II reconstructions were obtained from particles treated with 1 mM glutamate. Volume was calculated from densities filtered according to the FSC = 0.5 resolution criterion. FSC, Fourier shell correlation.
*Type IIa is the upper reconstruction in Fig. 2b.
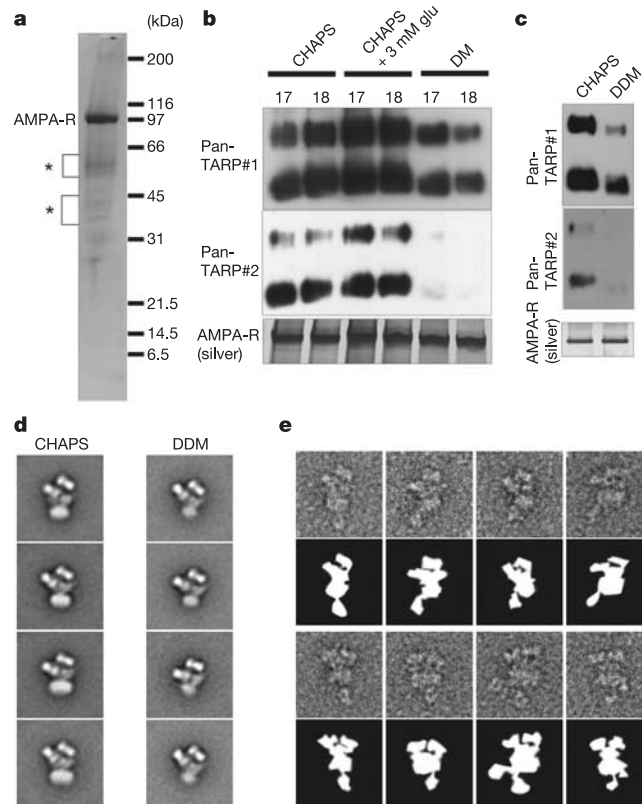†Type IIb is the lower reconstruction in Fig. 2b.

Figure 3 TARP contributes to the density of the transmembrane domain. **a**, Coomassie-blue-stained SDS–PAGE (10–20% gradient gel) of a concentrated AMPA-R preparation. Asterisks indicate bands containing γ-2/stargazin, γ-3, γ-4 and γ-8. **b**, Immunopurified AMPA-Rs after gel filtration in buffer containing CHAPS, CHAPS plus 3 mM glutamate, or decyl maltoside (DM). Fractions 17 and 18 were immunoblotted with two different pan-TARP antibodies. Silver staining of the purified AMPA-Rs in each lane is shown below. **c**, AMPA-Rs after gel filtration in buffer containing CHAPS or dodecyl maltoside (DDM) were immunoblotted as in **b**. Silver staining of the purified AMPA-Rs in each lane is shown below. **d**, Representative class averages of negatively stained type I AMPA-Rs purified with CHAPS (left column) versus DDM (right column). **e**, Labelling of AMPA-R particles purified in CHAPS with Fab fragments against a C-terminal peptide of TARP (pan-TARP#1 antibody). Schematic representation is shown below the raw electron microscopy image.
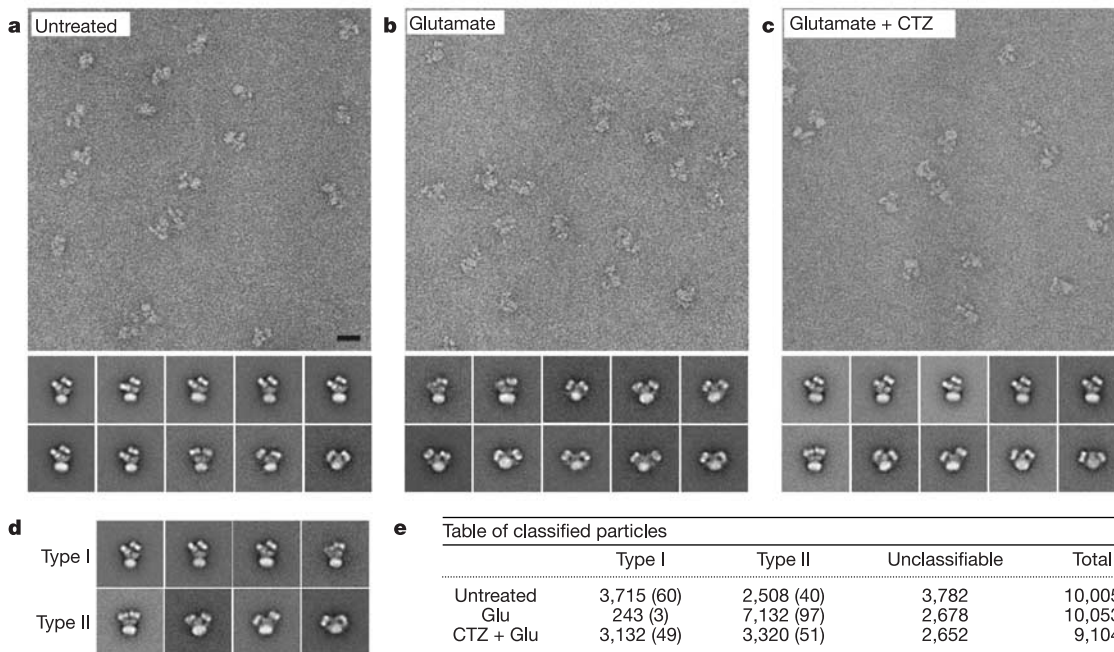

Table of classified particles

	Type I	Type II	Unclassifiable	Total
Untreated	3,715 (60)	2,508 (40)	3,782	10,005
Glu	243 (3)	7,132 (97)	2,678	10,053
CTZ + Glu	3,132 (49)	3,320 (51)	2,652	9,104

Figure 4 Ligand-dependent conformational change of AMPA receptors.
a–c, Micrographs and representative class averages of untreated AMPA-Rs (**a**), and AMPA-Rs treated with 1 mM glutamate (**b**) or 1 mM glutamate plus 330 μM cyclothiazide (CTZ) (**c**). Scale bar, 20 nm. **d**, Class averages of representative type I and type II conformations. The size of the panels in **d** and insets in **a–c** is 50 × 50 nm.
e, Quantification of the prevalence of AMPA-Rs in type I or type II conformations for the indicated conditions. Numbers in parentheses indicate percentage of classifiable particles in type I or type II conformation.

1 mM glutamate (Fig. 4b): only ~3% were type I, whereas ~97% were now type II. Thus, glutamate binding caused the two NTD dimers to separate. When treated with 1 mM glutamate plus 330 μM cyclothiazide (Fig. 4c), we observed a large increase in the prevalence of type I particles (~49%) compared with AMPA-Rs exposed to glutamate alone (~3%). These results imply that the different conformational states of AMPA-R particles are related to different functional states of the ligand-gated ion channel. However, even in the presence of cyclothiazide about one-half of the receptors assumed the type II conformation. The subpopulation of particles that adopt the type II conformation even in the presence of cyclothiazide may represent AMPA-R flop splice variants, which are less sensitive to cyclothiazide[25]. Because the type II conformation is seen in untreated preparations as well, it may also represent another, ligand-free functional state unrelated to desensitization. Our results suggest that the type I conformation represents both the putative ion-conducting and the ligand-free state of AMPA-R. The structural differences between these two states seem to be too subtle to be visualized at our current resolution.

In contrast to the density map of the homotetrameric GluR2 (ref. 3), which has been shown to have little conductivity[26], our three-dimensional reconstructions of native heterotetrameric AMPA-Rs showed prominent asymmetry at the NTD level. The consistency of our maps with the raw images, projection averages, and the shapes and sizes of the known crystal structures suggests that the asymmetry in the heterotetramer is real. Although uncommon, structural asymmetry, even in homo-oligomeric molecules, has been observed before[27], and in the case of AMPA-Rs the observed asymmetry could easily be accommodated by the flexibility of the linker sequences connecting the NTD and LBD domains.

The function of the NTDs is largely unknown. They are unnecessary for channel activity[28], but have been suggested to have a role in the subunit-specific assembly of AMPA-Rs[29] and in signalling during dendritic spine morphogenesis[30]. The gross conformational changes associated with glutamate binding might serve as a switch to trigger or terminate the putative signalling event. In other words, activated AMPA-Rs not only generate EPSCs but might also present a signal (a conformational change) of their own desensitization to the extracellular space. □

Methods

Purification of AMPA-R and Fab labelling
Details are provided in the Supplementary Information.

Specimen preparation and electron microscopy
Uranyl formate (0.7% w/v) was used for negative staining and cryo-negative staining as described[16]. Images were recorded using a Tecnai T12 (FEI/Philips) electron microscope equipped with a LaB$_6$ filament and operated at an acceleration voltage of 120 kV. For specimens prepared by conventional negative staining, images were taken at a magnification of ×52,000 using a defocus value of −1.5 μm. Grids of cryo-negatively stained specimens, used to collect image pairs of 50°/0° tilted specimens, were loaded on an Oxford cryo-transfer holder and maintained at liquid nitrogen temperature (below −160 °C) during image acquisition. Images were taken at a magnification of × 42,000 and a defocus value of −1.5 μm for images of the untilted specimens and −1.8 μm for 50° tilted specimens. All images were taken using low-dose procedures on Kodak SO-163 film and developed for 12 min with full-strength Kodak D-19 developer at 20 °C.

Image processing
Details are provided in the Supplementary Information.

1. Malinow, R. & Malenka, R. C. AMPA receptor trafficking and synaptic plasticity. *Annu. Rev. Neurosci.* **25,** 103–126 (2002).
2. Wollmuth, L. P. & Sobolevsky, A. I. Structure and gating of the glutamate receptor ion channel. *Trends Neurosci.* **27,** 321–328 (2004).
3. Tichelaar, W., Safferling, M., Keinanen, K., Stark, H. & Madden, D. R. The Three-dimensional structure of an ionotropic glutamate receptor reveals a dimer-of-dimers assembly. *J. Mol. Biol.* **344,** 435–442 (2004).
4. Keinanen, K. *et al.* A family of AMPA-selective glutamate receptors. *Science* **249,** 556–560 (1990).
5. Hollmann, M., O'Shea-Greenfield, A., Rogers, S. W. & Heinemann, S. Cloning by functional expression of a member of the glutamate receptor family. *Nature* **342,** 643–648 (1989).
6. Safferling, M. *et al.* First images of a glutamate receptor ion channel: oligomeric state and molecular dimensions of GluRB homomers. *Biochemistry* **40,** 13948–13953 (2001).
7. Rosenmund, C., Stern-Bach, Y. & Stevens, C. F. The tetrameric structure of a glutamate receptor channel. *Science* **280,** 1596–1599 (1998).
8. Chen, G. Q., Cui, C., Mayer, M. L. & Gouaux, E. Functional characterization of a potassium-selective prokaryotic glutamate receptor. *Nature* **402,** 817–821 (1999).
9. Wenthold, R. J., Petralia, R. S., Blahos, J. II & Niedzielski, A. S. Evidence for multiple AMPA receptor complexes in hippocampal CA1/CA2 neurons. *J. Neurosci.* **16,** 1982–1989 (1996).
10. Armstrong, N. & Gouaux, E. Mechanisms for activation and antagonism of an AMPA-sensitive glutamate receptor: crystal structures of the GluR2 ligand binding core. *Neuron* **28,** 165–181 (2000).
11. Sobolevsky, A. I., Yelshansky, M. V. & Wollmuth, L. P. The outer pore of the glutamate receptor channel has 2-fold rotational symmetry. *Neuron* **41,** 367–378 (2004).
12. Horning, M. S. & Mayer, M. L. Regulation of AMPA receptor gating by ligand binding core dimers. *Neuron* **41,** 379–388 (2004).
13. Stern-Bach, Y. *et al.* Agonist selectivity of glutamate receptors is specified by two domains structurally related to bacterial amino acid-binding proteins. *Neuron* **13,** 1345–1357 (1994).
14. Hollmann, M., Maron, C. & Heinemann, S. N-glycosylation site tagging suggests a three transmembrane domain topology for the glutamate receptor GluR1. *Neuron* **13,** 1331–1343 (1994).
15. Bennett, J. A. & Dingledine, R. Topology profile for a glutamate receptor: three transmembrane domains and a channel-lining reentrant membrane loop. *Neuron* **14,** 373–384 (1995).
16. Ohi, M., Li, Y., Cheng, Y. & Walz, T. Negative staining and image classification—powerful tools in modern electron microscopy. *Biol. Proc. Online* **6,** 23–34 (2004).
17. Frank, J. *Three-dimensional Electron Microscopy of Macromolecular Assemblies* (Academic, San Diego, 1996).
18. Kunishima, N. *et al.* Structural basis of glutamate recognition by a dimeric metabotropic glutamate receptor. *Nature* **407,** 971–977 (2000).
19. Armstrong, N., Sun, Y., Chen, G. Q. & Gouaux, E. Structure of a glutamate-receptor ligand-binding core in complex with kainate. *Nature* **395,** 913–917 (1998).
20. Sun, Y. *et al.* Mechanism of glutamate receptor desensitization. *Nature* **417,** 245–253 (2002).
21. Doyle, D. A. *et al.* The structure of the potassium channel: molecular basis of K$^+$ conduction and selectivity. *Science* **280,** 69–77 (1998).
22. Chen, L. *et al.* Stargazin regulates synaptic targeting of AMPA receptors by two distinct mechanisms. *Nature* **408,** 936–943 (2000).
23. Tomita, S., Fukata, M., Nicoll, R. A. & Bredt, D. S. Dynamic interaction of stargazin-like TARPs with cycling AMPA receptors at synapses. *Science* **303,** 1508–1511 (2004).
24. Patneau, D. K., Vyklicky, L. Jr & Mayer, M. L. Hippocampal neurons exhibit cyclothiazide-sensitive rapidly desensitizing responses to kainate. *J. Neurosci.* **13,** 3496–3509 (1993).
25. Sommer, B. *et al.* Flip and flop: a cell-specific functional switch in glutamate-operated channels of the CNS. *Science* **249,** 1580–1585 (1990).
26. Swanson, G. T., Kamboj, S. K. & Cull-Candy, S. G. Single-channel properties of recombinant AMPA receptors depend on RNA editing, splice variation, and subunit composition. *J. Neurosci.* **17,** 58–69 (1997).
27. Goodsell, D. S. & Olson, A. J. Structural symmetry and protein function. *Annu. Rev. Biophys. Biomol. Struct.* **29,** 105–153 (2000).
28. Pasternack, A. *et al.* Alpha-amino-3-hydroxy-5-methyl-4-isoxazolepropionic acid (AMPA) receptor channels lacking the N-terminal domain. *J. Biol. Chem.* **277,** 49662–49667 (2002).
29. Ayalon, G. & Stern-Bach, Y. Functional assembly of AMPA and kainate receptors is mediated by several discrete protein-protein interactions. *Neuron* **31,** 103–113 (2001).
30. Passafaro, M., Nakagawa, T., Sala, C. & Sheng, M. Induction of dendritic spines by an extracellular domain of AMPA receptor subunit GluR2. *Nature* **424,** 677–681 (2003).